Blends of Polybenzimidazole and Poly(vinylidene fluoride) for Use in a Fuel Cell

Dhamodaran Arunbabu, Arindam Sannigrahi, and Tushar Jana*

School of Chemistry, University of Hyderabad, Hyderabad, India

Received: October 3, 2007; In Final Form: February 3, 2008

We report a new blend system consisting of an amorphous polymer polybenzimidazole (PBI) and a semicrystalline polymer poly(vinylidene fluoride) (PVDF). A systematic investigation of the blend pair in various compositions using Fourier transform infrared (FT-IR) spectroscopy provides direct evidence of specific hydrogen bonding interaction involving the N−H groups of PBI and the $>CF_2$ groups of PVDF. Blending shows a maximum 30 cm^{-1} frequency shift in the N−H stretching band of PBI and also the existence of a partial double bond character in the PVDF chain. Differential scanning calorimetry (DSC) study proves the miscibility of these polymers in a wider composition range. The decrease of the T_g with increasing PVDF in the blend and also the decrease of both the T_m and T_c with increasing PBI in the blend attribute the miscibility of the blend systems. The PA doping level of the blend membranes improves significantly as a result of the hydrophobic nature of the PVDF component.

Introduction

Recently, high-temperature polymer electrolyte membrane fuel cells (HT-PEMFCs) have received tremendous attention in the energy research community.[1] Phosphoric acid (PA)-doped polybenzimidazole (PBI) has emerged as a most promising candidate among the large number of various high-temperature polymer electrolyte membranes that have been developed and studied to date.[2−6] PA-doped PBI exhibits excellent proton conductivity at high temperatures up to 200 °C, low gas permeability, and nearly zero water drag coefficient.[7,8] The proton conductivity increases with increasing PA doping level of the membrane.[5,6] Therefore, the main hurdle to achieve the superior quality PA-doped PBI membrane is to enhance the acid doping level in the membrane without destroying the other properties of the polymer. Though a variety of efforts have been attempted to obtain the PA-doped PBI membranes,[4−8,9−12] indeed there is an opportunity to develop a new and novel PBI material that perhaps significantly improves the acid doping level. Polymer blending is the most frequently used way to overcome the shortcomings of an individual polymer and to develop new materials with desirable properties by combining the advantages of the individual components of two or more polymers. Therefore, in principle, the appropriate choice of PBI blend systems could enhance the proton conductivity of the PA-doped PBI blend membrane.

PBI has exceptional thermal and oxidative stability and fire retarding capacity, and it is widely used as a nonflammable fiber for high temperature application.[13] PBI is an amorphous polymer with a very high glass transition temperature.[13] It possesses both proton donor (−NH−) and proton acceptor (−N═) hydrogen-bonding sites, which exhibit specific interaction with polar solvents[14,15] and upon blending with a variety of polymers.[16−18] Various polymers possessing carbonyl and sulfonyl functionality in their backbone can easily take part in the specific interaction with the available hydrogen-bonding sites of the PBI chain and result in miscible blends. A large number of PBI blends with several polymers such as polyimide, poly(ether imide), sulfonated polysulfone, and so forth are studied in the literature by various authors in regards to the specific hydrogen bonding interactions involved between the proton donating (−NH−) site of PBI with the proton accepting site of the other polymers.[16−22]

Poly(vinylidene fluoride) (PVDF) is a semicrystalline hydrophobic polymer and known to forms miscible blends with a variety of polymers. Blends of PVDF with Nafion[23] and sulfonated poly(ether ether ketone)[24] are prepared for their potential use in a direct methanol fuel cell. There is a high probability of a strong interaction between the $>CF_2$ groups of PVDF and the N−H groups of PBI, which could develop a compatible blending of a PBI/PVDF pair. Moreover, we hypothesize that, because of the hydrophobic nature of the PVDF, the blend membrane cannot absorb moisture and thus can imbibe more acid, resulting in a better doping level. To our knowledge, until now there is no report on PBI/PVDF blends in the literature. In this note, we report the study of PBI/PVDF blend systems and their potential to be used as a proton exchange membrane in PEMFC.

Experimental Methods

Materials. Poly[2,2′-(*m*-phenylene)-5,5′-benzimidazole] (PBI) was synthesized in the laboratory using the method described earlier,[9,14] and the dried polymer has an inherent viscosity (IV) value of 0.526 dL/g in H_2SO_4 (98%) at 30 °C. PVDF was purchased from Aldrich having an weight average molecular weight (M_w) of 530 000. Dimethylacetamide (DMAc; HPLC grade) and PA (85%) were obtained from Merck (India) and used as received.

Blend Preparation. Blends were prepared by dissolving the two polymers (0.5% w/v) in DMAc at the required ratio for 24 h. The homogeneous blend solutions were filtered through a 0.5 μm PTFE membrane and then poured into a glass Petri dish at 80 °C to cast the blend films. Transparent homogeneous thin films (20−40 μm) were boiled in water thoroughly and dried in a vacuum oven at 100 °C for 3 days to remove the solvent completely. The absence of a 2940 cm^{-1} peak in the IR spectrum of the blend samples ensures the complete removal of DMAc.

* To whom correspondence should be addressed. Tel: (91) 40 23134808. Fax: (91) 40 23012460. E-mail: tjsc@uohyd.ernet.in or tjscuoh@gmail.com.

10.1021/jp711860v CCC: $40.75
Published on Web 04/08/2008

Characterization Techniques. Fourier transform infrared (FT-IR) spectra of the thin blend films were recorded on a Nicolet 5700 FTIR spectrometer at a resolution of 0.5 cm^{-1} with an average of 32 scans. A differential scanning calorimeter (Pyris Diamond DSC, Perkin-Elmer) was used to study the thermal transitions of the blend samples. The DSC was calibrated using standard In and Zn before the samples were scanned. Blend samples were annealed at 450 °C (100/0, 90/10, 75/25, and 50/50) or at 400 °C (25/75 and 10/90) for 20 min, cooled to 50 °C at a cooling rate of 200 °C/min, and subsequently (after 30 min equilibration at 50 °C) scanned from 50 °C to 450 °C/400 °C at a heating rate of 40 °C/min. In the case of cooling experiments, the 450 °C/400 °C annealed samples were scanned from 450 °C/400 °C to 50 °C at a scan rate of 5 °C/min. The atomic force microscope (AFM) images of the samples were captured in an AFM apparatus (model: Solver Pro M of NT-MDT) working in semi-contact mode. A microcantilever with a spring constant of 10 N/m was used to scan the samples. A small portion of blend samples (thin films) were fixed on a glass substrate and then imaged in AFM.

PA Doping, Water Uptake, and Swelling Ratio. The dried membranes were immersed into PA (85%) for 3 days and then titrated against NaOH using an Autotitrator (Metrohm 702). The PA doping level was calculated as the number of PA mols present per PBI repeat unit.[5] Water uptake and swelling ratio of the membranes were obtained by immersing the membranes in water for 3 days. The blend membranes were thoroughly vacuum-dried for 3 days at 100 °C. The length and weight of the membrane were measured. Then the membranes were immersed in water for 3 days at room temperature. The wet membranes were quickly wiped to remove the surface water. Again the length and weight of the wet membrane were noted. Water uptake values of the membranes were calculated as

$$\text{Water Uptake} = \frac{W_w - W_d}{W_d} \times 100\%$$

where W_w and W_d are the weights of the wet and dry membranes, respectively. The swelling ratios of the membranes were calculated as

$$\text{Swelling Ratio} = \frac{L_w - L_d}{L_d} \times 100\%$$

where L_w and L_d are the lengths of the wet and dry membranes, respectively. The PA doping level, water uptake and swelling ratio measurements of the membranes were carried out in triplicate independently with different pieces of membranes to check the reproducibility of the results, and the average values are presented in Table 2.

Results and Discussion

FT-IR Study. The blending of PBI and PVDF in various compositions is studied thoroughly using FT-IR spectroscopy. Previously, the interactions and miscible behaviors in PBI blends had been examined extensively by FT-IR spectroscopy in the literature.[16−20] It was established that the most valuable information can be obtained and interpreted from the N−H stretching region of the PBI. The spectrum of PBI shows a series of N−H stretching bands in the 3600−3030 cm^{-1} region,[21] and, moreover, PVDF does not have any distinct vibrational frequency in this region (Supporting Information, Figure 1). This creates a PVDF-free window in the 3600−3030 cm^{-1} region, allowing us to monitor any change in the N−H stretching frequencies very precisely due to the blending of PBI with PVDF. The reason for the miscibility of the two polymers is investigated in terms of the specific hydrogen bonding interaction between the −NH group of the imidazole moiety of the PBI chains and the $>CF_2$ groups of the PVDF chains by analyzing the frequency shifts of the N−H stretching region. The N−H stretching region can be separated into at least three distinguishable contributions as shown in Figure 1 of the Supporting Information as follows: (i) a relatively sharp peak at 3420 cm^{-1} due to isolated, non-hydrogen-bonded free N−H groups; (ii) a very broad asymmetric peak centered at around 3144 cm^{-1} owing to self-associated, hydrogen-bonded N−H groups; and (iii) a third low-intensity peak at 3063 cm^{-1} due to the stretching modes of the aromatic C−H groups.[17,21] The FT-IR spectra of PBI and some representative blends of PBI with PVDF in the 3600−3030 cm^{-1} region are presented in Figure 1. From the figure it is evident that the free non-hydrogen-bonded N−H stretching band at 3420 cm^{-1} displays a substantial broadening and displacement to lower frequencies with increasing PVDF content in the blends. In the case of 50/50 blends, the free N−H band appears at 3390 cm^{-1}. However, the C−H aromatic stretching at 3063 cm^{-1} does not change its position. The red shift and peak broadening of the free N−H band upon blending indicates the formation of hydrogen bonding between the imidazole ring of the PBI and the $>CF_2$ groups of the PVDF. A more careful analysis of Figure 1 reveals that, with increasing PVDF content in the blends, the intensity of the self-associated hydrogen-bonded N−H band centered at 3144 cm^{-1} diminishes, and a new broad band becomes visible, centered at around 3190 cm^{-1}. This frequency shift can be attributed to the weakening of self-associated N−H−N hydrogen bonding of the PBI chains and the formation of hydrogen bonding with the PVDF chains. Similar types of observations are reported in various blend systems of PBI with sulfonated polysulfone, polyimide, poly(ether imide), and so forth.[16−20] A maximum 30 cm^{-1} wavenumbers displacement of the free N−H stretching band is observed at about 50% PVDF blend, after which a plateau value is reached (Figure 2). The most notable feature in Figure 2 is that the N−H stretching band of PBI at 3420 cm^{-1} has shifted

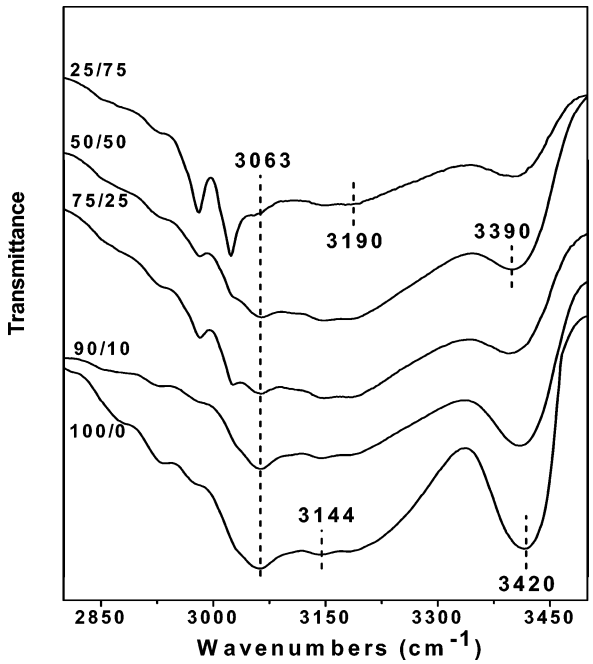

Figure 1. FT-IR spectra of the PBI/PVDF blend film samples at their indicated compositions.

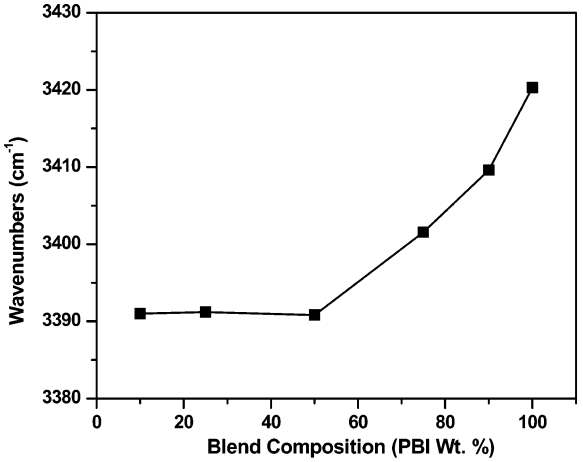

Figure 2. Variation of the N−H stretching frequencies of PBI as a function blend composition.

significantly to a lower wavenumber (3390 cm^{-1}) up to 50% PVDF, then it saturates and does not move further to the lower wavelength with further incorporation of PVDF in the blend. This behavior implies that the interaction in the blend is stoichiometric in nature between the functional groups of the two polymers.

Certainly, the previous section clearly proves the presence of specific interaction between the two polymer components in this blend system and its effect on the N−H stretching frequencies. In principle, we should also obtain some sort of changes in the vibrational frequencies of the PVDF component in the blends due to the interaction between the $>CF_2$ of PVDF and the N−H of PBI. However, it is quite difficult to identify the PVDF frequencies in the blend systems, especially in the lower wavenumber region, because of the overlapping of the PBI peaks. Therefore, we look into the lower wavenumber region of the IR spectra very carefully by digitally subtracting the spectrum from that of the pure PBI. The peak at 1402 cm^{-1} in pure PVDF (Figure 3A) represents the characteristic frequencies of C−C, C−C−H, and H−C−H bonds. Similarly, the peaks at 1179 cm^{-1} and 882 cm^{-1} in pure PVDF (Figure 3B,C) are due to the vibrational frequencies of C−F, C−C−F, and F−C−F bonds.[25] From Figure 3A, it is clearly visible that the 1402 cm^{-1} peak of pure PVDF shifts gradually toward higher frequency with increasing PBI content in the blends and reaches 1416 cm^{-1} for a 90% PBI sample. This observation can be attributed to the enhancement of the C−C bond strength.[25] On the other hand, the peak positions at 1179 cm^{-1} and 882 cm^{-1} in pure PVDF show displacement toward lower frequency with increasing PBI content in the blends (Figure 3B,C). Though

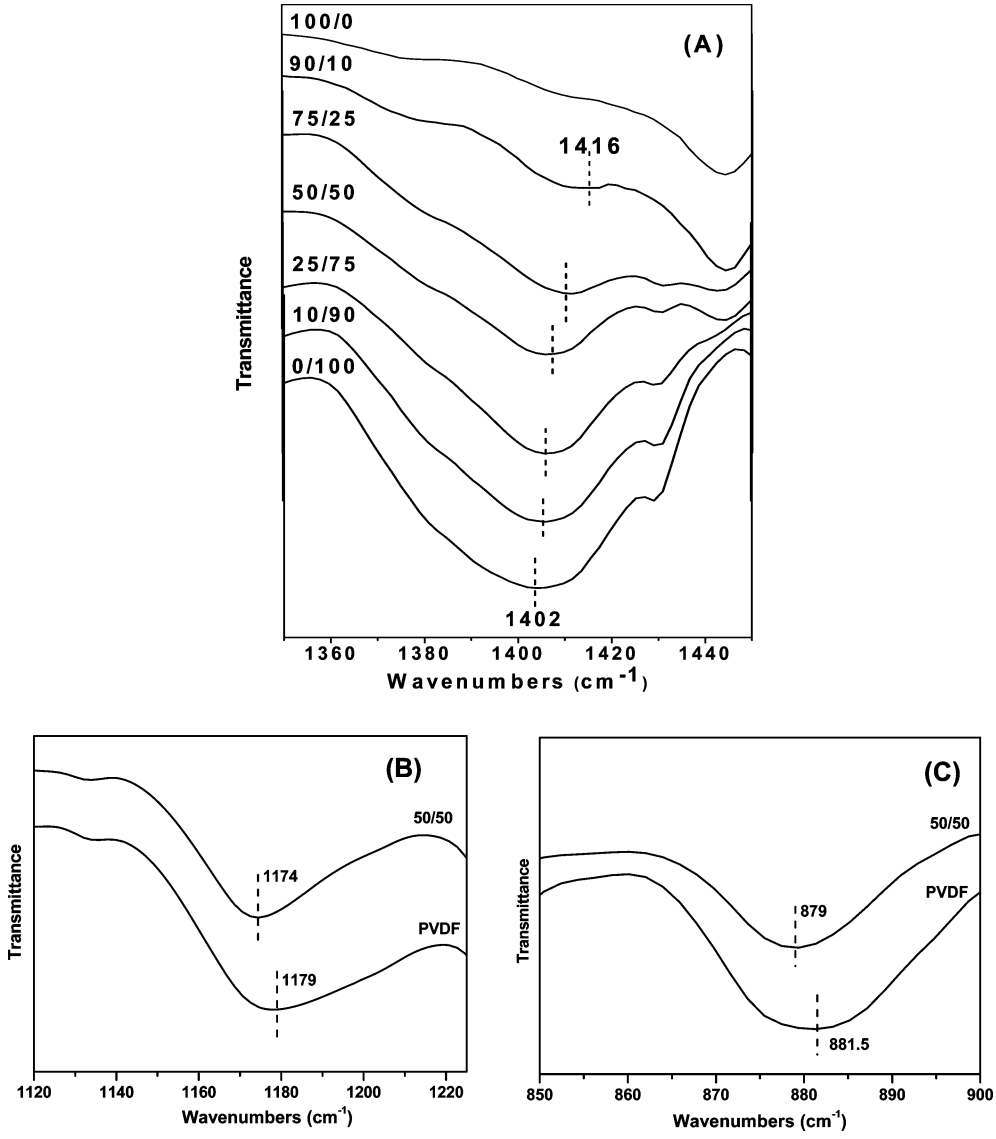

Figure 3. FT-IR spectra of the PBI/PVDF blend films at their indicated compositions.

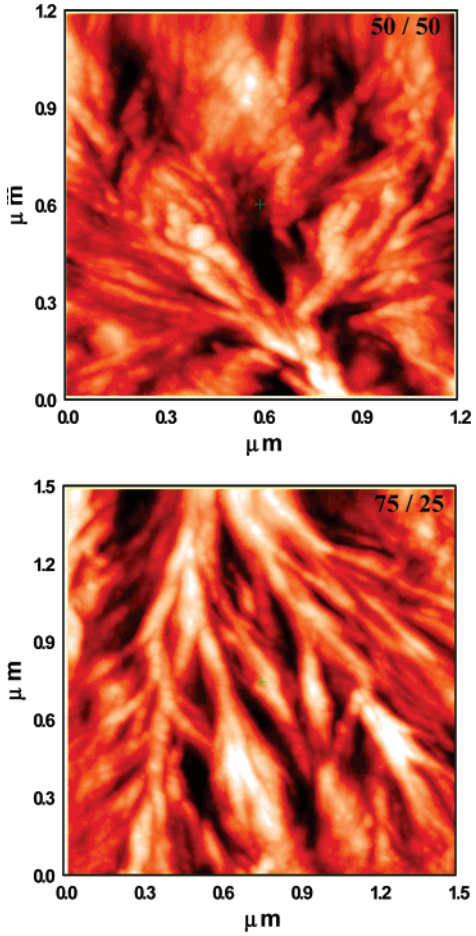

Figure 4. AFM images of the representative blend samples.

the shifts are very small, it is clearly visible and within the instrument resolution. These observations indicate the weakening of the C−F bond.[25] In summary, considering all the IR data, it can be concluded that, because of the specific hydrogen bonding interaction between the N−H of PBI and the $>CF_2$ of PVDF, the C−F bond becomes weaker and elongated, and hence the F atom cannot pull all the electrons from the C−F bond, which results in better conjugation along the C−C bond and creates a partial double-bond character in PVDF. Therefore it is obvious that the hydrogen bonding between PBI and PVDF is the key factor for the miscibility of this blend system.

Thermodynamical Study. All the thin blend films studied here are homogeneous, indicating the miscibility of the two polymers. The surface morphologies of the blends probed by AFM show the spherulitic morphology. These spherulites are observed because of the PVDF component in the blends. Figure 4 shows the representative AFM images of the different blend samples. The characteristic Maltese cross-pattern of the spherulites and the oriented arms of the cross are clearly visible in the Figure 4.[26] Along with the IR studies discussed earlier, the miscibility study of the PBI−PVDF blends are verified by differential scanning calorimetric study. DSC experiments show that the glass transition temperature (T_g) of PVDF is −44 °C, and that of PBI is 433 °C. Also, PVDF shows a crystalline melting temperature (T_m) at 161 °C and a crystallization temperature (T_c) at 134 °C. Despite the large difference in T_g's of the two components, we are able to study the blend's miscibility by measuring the T_g of the blend as it is usually done in case of miscible blend systems. The DSC thermograms showing the T_g are presented in the Supporting Information, Figure 2. This Figure shows that only blends containing less

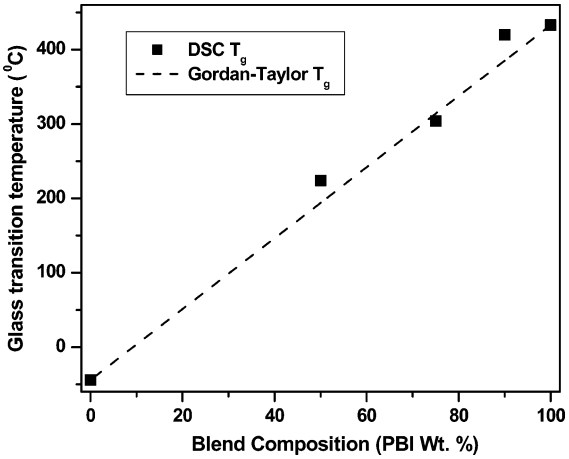

Figure 5. Variation of the glass transition temperature (T_g) of PBI as a function of blend composition. The solid points (■) are the experimentally obtained T_g from the DSC study, and the dotted line (---) is the calculated T_g curve according to the Gordon−Taylor equation with $k = 1$.

than or equal to (≤) 50% PVDF (w/w) can yield a single T_g. The resulting glass transition temperature of the blends varies with the overall blend composition, as indicated by the filled square in Figure 5. The presence of a single and compositional dependent T_g indicates that the blend exhibits a homogeneous single phase. This implies that the two polymers are miscible. The decrease of the T_g of the blend with increasing PVDF content is expected because of the interaction between the PBI and the PVDF. As a result of such specific interaction, the PVDF chains force the PBI chains to begin their segmental motions at lower temperature, and hence the T_g decreases. It is worthwhile to note from Figure 5 that the T_g of the blend has dramatically decreased up to 50% PVDF, and then no T_g is observed with further increase of PVDF content in the blend. This observation is in agreement with our IR results discussed in the previous section (Figure 2). Hence, DSC studies as well as IR studies prove that the interaction between the functional groups of the two components in the blend is stoichiometric in nature. The dependence of T_g on the blend composition can be evaluated by utilizing the well-known Gordon−Taylor equation[27]

$$T_g = \frac{W_1 T_{g1} + k W_2 T_{g2}}{W_1 + k W_2} \quad (1)$$

where W is the weight fraction, T_g is the glass transition temperature of the blends, T_{g1} and T_{g2} are those of the pure components, PBI and PVDF, respectively, and k is an adjustable fitting parameter (Gordon−Taylor constant) that describes the strength of the intermolecular interaction between the components in miscible polymer blends. Good miscibility of the two polymer components is achieved when the value of $k = 1$. The dotted line in Figure 5 is drawn using the Gordon−Taylor equation with $k = 1$. The dotted line fits well with the experimental points in Figure 5. This can be attributed to the strong intermolecular interaction between the two polymer components (PBI and PVDF) in the blends, which yields the miscible blends of PBI and PVDF.

We have observed a single glass transition temperature of the blends up to 50% PVDF, which varies with the overall blend compositions (Figure 5). These blends (up to 50% PVDF) do not show any melting endotherm (T_m) and crystallization exotherm (T_C). In contrast, blends containing greater than 50%

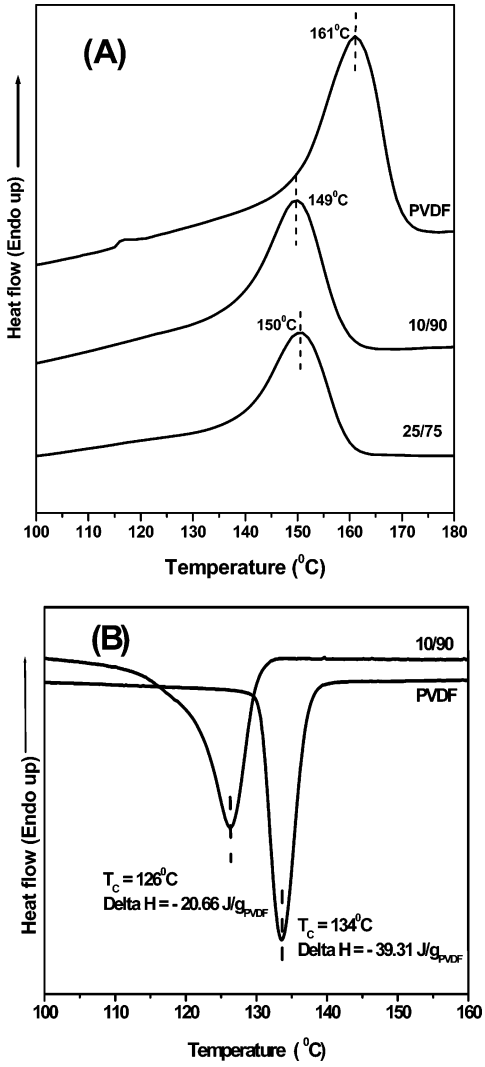

Figure 6. The (A) T_m and (B) T_c of the PBI/PVDF blends at their indicated blend compositions.

PVDF do not show any T_g, but they show both melting endotherm and crystallization exotherm, as observed from Figure 6. Figure 6A,B shows that both the T_m and the T_c of the blends are lower than that of neat PVDF. These depressions in the crystalline melting temperature (T_m) and the crystallization temperature (T_c) indicate the occurrence of intermolecular interaction between the PVDF and the PBI, which hinders the formation of crystal of the crystalline component, PVDF.[24,28] The crystallinity index of the blend samples is calculated from the following equation:

$$X_c = \frac{\Delta H_f}{\Delta H_f^0} \tag{2}$$

where $\Delta H_f^0 = 104.6$ J/g is the heat of fusion of 100% crystalline PVDF,[29] and ΔH_f is the heat of fusion of the samples obtained from the DSC heating endotherms. The obtained data are tabulated in Table 1. A better evidence of the hindered crystallization process in the blend can be realized from the Figure 6B and Table 1. The crystallinity index (X_c) has significantly reduced in the case of the blend samples. Hence, all these results indicates that the crystallization of the blends (containing greater than 50% PVDF) has been considerably perturbed by the PBI. Therefore the PBI has to be present in the PVDF crystal to create the perturbation in the PVDF crystallization. This implies that, because of the interaction with the PBI, all the PVDF chains may not able to get close and form crystals. Therefore, considering all the DSC results, it can be concluded that the two components (PBI and PVDF) in the blend are mixed together with a high miscibility. Wang et al. have observed a similar kind of miscible behavior from the DSC studies in crystalline/amorphous blends of poly(caprolactone)/poly(4-vinylphenol).[30]

TABLE 1: Thermodynamical Data Obtained from the DSC Studies of PBI/PVDF Blends

PBI/PVDF	ΔH_f (J/g_{blend})	ΔH_f (J/g_{PVDF})	X_C (PVDF) (%)
25/75	12.02	16.03	15.33
10/90	19.30	21.44	20.49
0/100	36.44	36.44	34.84

TABLE 2: Water Uptake, Swelling Ratio, and PA Doping Level of the PBI/PVDF Blend Membranes

PBI/PVDF (wt %)	water uptake (wt %)	swelling ratio (%)	PA mols/ PBI repeat unit
100/0	12.98	5.62	10.26
90/10	11.01	3.18	11.85
75/25	9.68	3.87	16.88
50/50	9.07	3.54	12.60
25/75	3.11	1.84	5.92
10/90	3.08	1.52	5.49
0/100	2.70	0.692	0.06[a]

[a] In the case of 100% PVDF, the data represents PA mols/PVDF repeat unit.

PA Loading. The PA loading capacity of the membrane has great effects on the properties of PEMFC. In general, higher acid loading is desirable to achieve the most efficient PEMFC.[5,6] Higher acid content facilitates the transport of the protons, which significantly improves the fuel cell efficiency.[5,6] The PA doping level of the membrane is expressed as the number of PA moles per PBI repeat unit. Generally, very low PA doping level (~10 mols/PBI repeat unit) values are reported. Previously, we reported that the PBI membrane made from the PBI gel in PA shows a very high PA doping level: 35−40 mols PA per PBI repeat unit.[9] The proton conduction of the acid-doped PBI membrane does not depend on the amount of water present in it; rather PBI exhibits nearly zero osmotic drag coefficient.[4,7,8] However, it is also well-known that PBI is a good desiccant, and it absorbs moisture very easily.[5,6] Since PBI molecule possesses a proton-accepting nitrogen (−N═) atom in the backbone, it can easily absorb moisture, which partially blocks the acid molecule from doping the PBI chains. Hence there is always a competition between the water and the acid molecules, and finally they reach a compromise. However, if by some means the water uptake capacity of the membrane can be reduced, that will help the membrane to load more PA. Since PVDF is a hydrophobic polymer, the PBI/PVDF blend membrane should have less water uptake than pure PBI. Table 2 shows that both the water uptake and the swelling ratio of the blend membranes are suppressed with increasing PVDF in the blends. Table 2 data shows that, as the water uptake decreases, the PA doping level of the membrane increases. For high PVDF content blends (>50%), the decrease of PA doping level is obvious since PVDF cannot hold the PA. Therefore, from the above results, it seems obvious that blending of the PBI with the PVDF enhances the PA doping level.

Conclusion

New blend systems of PBI with hydrophobic PVDF at various compositions have been prepared using the solution casting

method, and the blends are characterized by FT-IR, DSC, AFM, water uptake, and PA doping level studies. FT-IR studies of the blends reveal the presence of specific hydrogen bonding interaction between the N−H of PBI and the $>CF_2$ of PVDF, and this results in the miscibility of the PBI and the PVDF. The homogeneity and spherulitic morphology of the blend films suggest the miscibility of PBI and PVDF and hence validate our argument from the FT-IR analysis. The miscibility of the blends has been established by analyzing the single T_g and composition-dependent T_g criterion. DSC studies of the blend clearly demonstrate that, because of the specific intermolecular interaction between the two components, the depression of the T_g of the blends containing $\leq$50% PVDF and the T_m and T_c of the blends containing greater than 50% PVDF takes place. The hindrance to the crystallization of the PVDF-enriched blend samples due to the blending is also evident from the reduced crystallinity. Finally, the enhancement of the PA doping level of the blend membrane compared to that of pure PBI is observed since the hydrophobic PVDF suppresses the water uptake capacity of the materials and hence allows the acid to interact more efficiently with the PBI backbone.

Acknowledgment. We gratefully acknowledge the financial support by the DST (Fast Track Grant No. SR/FTP/CS-49/2005). D.A. thanks UGC for providing the junior research fellowship during this work.

Supporting Information Available: Figures showing the FT-IR spectra of PBI and PVDF films and DSC thermograms of the blend samples. This material is available free of charge via the Internet at http://pubs.acs.org.

References and Notes

(1) Blomen, L. J. M. J. *Fuel Cell Systems*; Plenum Press, New York, 1993.
(2) Hickner, M. A.; Ghassemi, H.; Kim, S. Y.; Einsla, B. R.; McGrath, J. E. *Chem. Rev.* **2004**, *104*, 4587.
(3) Roziere, J.; Jones, D. J. *Annu. Rev. Mater. Res.* **2003**, *33*, 503.
(4) Savinell, R.; Yeager, E.; Tryk, D.; Landau, U.; Wainright, J.; Weng, D.; Lux, K.; Litt, M.; Rogers, C. *J. Electrochem. Soc.* **1994**, *141*, L46.
(5) Xiao, L.; Zhang, H.; Jana, T.; Scanlon, E.; Chen, R.; Choe, E.-W.; Ramanathan, L. S.; Yu, S.; Benicewicz, B. C. *Fuel Cells* **2005**, *5*, 287.
(6) Xiao, L.; Zhang, H.; Scanlon, E.; Ramanathan, L. S.; Choe, E.-W.; Rogers, D.; Apple, T.; Benicewicz, B. C. *Chem. Mater.* **2005**, *17*, 5328.
(7) Samms, S. R.; Wsmus, S.; Savinell, R. F. *J. Electrochem. Soc.* **1996**, *143*, 1225.
(8) Weng, D.; Wainright, J. S.; Landau, U.; Savinell, R. F. *J. Electrochem. Soc.* **1996**, *143*, 1260.
(9) Sannigrahi, A.; Arunbabu, D.; Jana, T. *Macromol. Rapid Commun.* **2006**, *27*, 1962.
(10) Mecerreyes, D.; Grande, H.; Miguel, O.; Ochoteco, E.; Marcilla, R.; Cantero, I. *Chem. Mater.* **2004**, *16*, 604.
(11) Weber, J.; Antonietti, M.; Thomas, A. *Macromolecules* **2007**, *40*, 1299.
(12) Jouanneau, J.; Mercier, R.; Gonon, L.; Gebel, G. *Macromolecules* **2007**, *40*, 983.
(13) Choe, E. W.; Choe, D. D. In *Polymeric Materials Encyclopedia*; Salamone, J. C., Ed.; CRC Press, New York, 1996.
(14) Sannigrahi, A.; Arunbabu, D.; Sankar, R. M.; Jana, T. *Macromolecules* **2007**, *40*, 2844.
(15) Shogbon, C. B.; Brousseau, J.-L.; Zhang, H.; Benicewicz, B. C.; Akpalu, Y. *Macromolecules* **2006**, *39*, 9409.
(16) Musto, P.; Karasz, F. E.; MacKnight, W. J. *Macromolecules* **1991**, *24*, 4762.
(17) Deimede, V.; Voyiatzis, G. A.; Kallitsis, J. K.; Qingfeng, L.; Bjerrum, N. J. *Macromolecules* **2000**, *33*, 7609.
(18) Wang, Y.; Goh, S. H.; Chung, T-S. *Polymer* **2007**, *48*, 2901.
(19) Ahn, T-K.; Kim, M.; Choe, S. *Macromolecules* **1997**, *30*, 3369.
(20) Guerra, G.; Choe, S.; Williams, D. J.; Karasz, F. E.; MacKnight, W. J. *Macromolecules* **1988**, *21*, 231.
(21) Musto, P.; Karasz, F. E.; MacKnight, W. J. *Polymer* **1993**, *34*, 2934.
(22) Liang, K.; Banhegyi, G.; Karasz, F. E.; MacKnight, W. J. *J. Polym. Sci., Part B: Polym Phys.* **1991**, *29*, 649.
(23) Kim, H. j.; Kim, H. J.; Shul, Y. G.; Han, H. S. *J. Power Sources* **2004**, *135*, 66.
(24) Xue, S.; Yin, G. *Polymer* **2006**, *47*, 5044.
(25) Urban, M. W.; Salazar-Rojas, E. M. *Macromolecules* **1988**, *21*, 372.
(26) Sperling, L. H. *Introduction to Physical Polymer Science*; John Wiley & Sons, Inc: New York, 1992.
(27) Gordon, M.; Taylor, J. S. *J. Appl. Chem.* **1952**, *2*, 495.
(28) Qiu, Z.; Yan, C.; Lu, J.; Yang, W.; Ikehara, T.; Nishi, T. *J. Phys. Chem. B* **2007**, *111*, 2783.
(29) Nakagawa, k.; Ishida, Y. *J. Polym. Sci. Polym. Phys.* **1973**, *11*, 2153.
(30) Wang, J.; Cheung, M. K.; Mi, Y. *Polymer* **2002**, *43*, 1357.